JCTC Journal of Chemical Theory and Computation

Accurate First-Principle Prediction of ^{29}Si and ^{17}O NMR Parameters in SiO_2 Polymorphs: The Cases of Zeolites Sigma-2 and Ferrierite

Alfonso Pedone,[†] Michele Pavone,[‡,§] Maria Cristina Menziani,[†] and Vincenzo Barone*[,‡,§,||]

Dipartimento di Chimica, Università di Modena e Reggio Emilia, Via G. Campi 183, 41100 Modena, Italy, Dipartimento di Chimica "Paolo Corradini" and CR-INSTM "Village", Università di Napoli Federico II, Complesso Universitario Monte Sant'Angelo Via Cintia I, 80126, Napoli, Italy, and Istituto per i Processi Chimico Fisici CNR and CR-INSTM "Village", Area della Ricerca del CNR Via Moruzzi 1, 56124 Pisa, Italy

Received July 29, 2008

Abstract: The magnetic shielding tensors of silica polymorphs have been investigated by means of quantum chemical calculations. Several levels of theory, from Hartree−Fock to the last generation of Density Functional Theory based approaches, have been tested on predicting ^{29}Si and ^{17}O isotropic and principal components of the chemical shift tensors together with ^{17}O quadrupolar coupling constants. The NMR parameters have been computed on all known silica systems, namely, α-quartz, α-cristobalite, coesite, Sigma-2, and ferrierite zeolites. Besides, cluster based approaches have been compared to a hybrid Quantum-Mechanics/Molecular-Mechanics (QM/MM) method, within the ONIOM scheme. The convergence of computed ^{17}O NMR parameters with respect to cluster size is found to be system-dependent. Excellent agreement between computed and experimental data has been found for ^{29}Si NMR parameters of the different Si sites of silica polymorphs and of Sigma-2 and ferrierite zeolites.

Introduction

Silicates are the major constituents of a large range of materials, from zeolites to clays, from minerals to glasses. These materials present very complex structural features: an accurate definition of their structure−property relationships is not always straightforward, although it is extremely important in both fields of technological industries and geosciences. For silicates, X-ray diffraction (XRD) and solid-state nuclear magnetic resonance (NMR) techniques provide the experimental framework to define the atomistic structural details of crystals (or powders) and the local chemical environment embedding specific sites, respectively. However, in some cases, when there are no chances to obtain single crystals or the different magnetically active sites present very similar chemical surroundings, the rationalization of experimental data could strongly benefit from theoretical modeling techniques able to predict reliable structural properties and accurate NMR parameters. This last issue is the focus of the present contribution.

The dominant constituents of silicates are silicon and oxygen atoms, both the elements present isotopes, ^{29}Si and ^{17}O, amenable of NMR studies. The ^{29}Si atom (nuclear spin equal to 1/2) has a relatively high natural abundance (4.7%), which allowed the accumulation of several ^{29}Si NMR data over the years for natural minerals, glasses, and zeolites.[1,2] Some empirical correlations between ^{29}Si chemical shifts and a number of structural parameters have been proposed: in particular, the coordination of Si atoms, the connectivity of SiO_4 tetrahedra, the Si−O bond length, and the Si−O−Si angle.[3−10] The ^{17}O atom has a nuclear spin equal to 5/2, and it is possible to measure the chemical shifts and

* Corresponding author e-mail: baronev@unina.it.
[†] Università di Modena e Reggio Emilia.
[‡] Università di Napoli Federico II.
[§] CR-INSTM "Village".
[||] IPCF-CNR.

10.1021/ct8003035 CCC: $40.75
Published on Web 10/30/2008

quadrupolar parameters. However, ^{17}O NMR technique is challenging for the low natural abundance (0.037%) of this oxygen isotope. Besides, being ^{17}O a quadrupolar nucleus, NMR peaks are broadened by electric quadrupolar interactions between the nuclear electric quadrupole and the electric field gradient (efg) at the nucleus. Thanks to enriched samples and to the development of high-resolution techniques, the amount of information from ^{17}O NMR spectra of silicates is rapidly increasing.[11−15] Nevertheless, the spectra are still very difficult to interpret, also because empirical correlations have not yet been proposed for enabling the assignment of chemical shifts to each site. Indeed, recent *ab initio* calculations by Xue et al.[16,17] on small silicate clusters showed that ^{17}O chemical shift is strongly affected by the size of the rings constituted by the Si−O−Si silicate network and by the puckering of the cluster where it resides. Moreover, it has been recently found that ^{17}O quadrupolar coupling constant (C_Q - *vide infra*) is strongly dependent on Si−O distance and Si−O−Si angle values, while the asymmetry parameter (η - *vide infra*) is dependent on Si−O−Si angle but not on Si−O distance.[18]

Under such circumstances, it is not hard to highlight how relevant is the accuracy of NMR *ab initio* calculations for allowing the assignment of each site in complex ^{29}Si- and ^{17}O NMR spectra of SiO_2-polymorphic systems. Most of the previous reports on this topic were restricted to calculation of isotropic shifts by using the Hartree−Fock (HF) level of theory on cluster models of silica polymorphs,[19] possible zeolite precursors,[20] and a number of different zeolites.[14,15,21] Brouwer et al.[22] first demonstrated that the principal components of zeolite ^{29}Si chemical shift (CS) tensors can be accurately calculated and used together with ultrahigh-field NMR experiments into an NMR crystallography structure refinement tool for zeolites.[23] The framework structure of Sigma-2 zeolite was solved from solid-state ^{29}Si NMR data and subsequently refined against the computed ^{29}Si CS tensors to give a NMR determined crystal structure that was in a very good agreement with the single-crystal XRD structure. The cluster model has also been used with success to calculate ^{1}H and ^{29}Si NMR chemical shifts of silane and silanol groups in silica[24,25] by employing the Density Functional Theory method with the hybrid B3LYP functional.[26,27] Moreover, periodic density functional theory (DFT-PBE) calculations on a number of silica polymorphs, including ferrierite and Faujasite zeolites, performed well[28] in the determination of the ^{29}Si and ^{17}O isotropic shifts and ^{17}O quadrupolar parameters. However, to our knowledge there is still the lack in recent literature of a systematic investigation able to verify the performance of different *ab initio* methods for computing ^{29}Si- and ^{17}O NMR parameters of silicates.

In the present paper, the accuracy of HF- and several DFT-based methods (PBE,[29,30] PBE0,[31] B3LYP,[26,27] CAM-B3LYP,[32] and M05−2X[33] - *vide infra*) for predicting magnetic parameters of α-quartz,[34] α-cristobalite,[35] coesite,[36] Sigma-2,[22] and ferrierite[37] all-silica zeolites has been tested. Besides, the effectiveness of a multiscale method, the ONIOM scheme,[38−40] which combines Quantum-Mechanics and Molecular Mechanics approaches (QM/MM) in order to account for long-range Coulombic interactions and to achieve convergence of computed properties with respect to cluster sizes has been investigated.

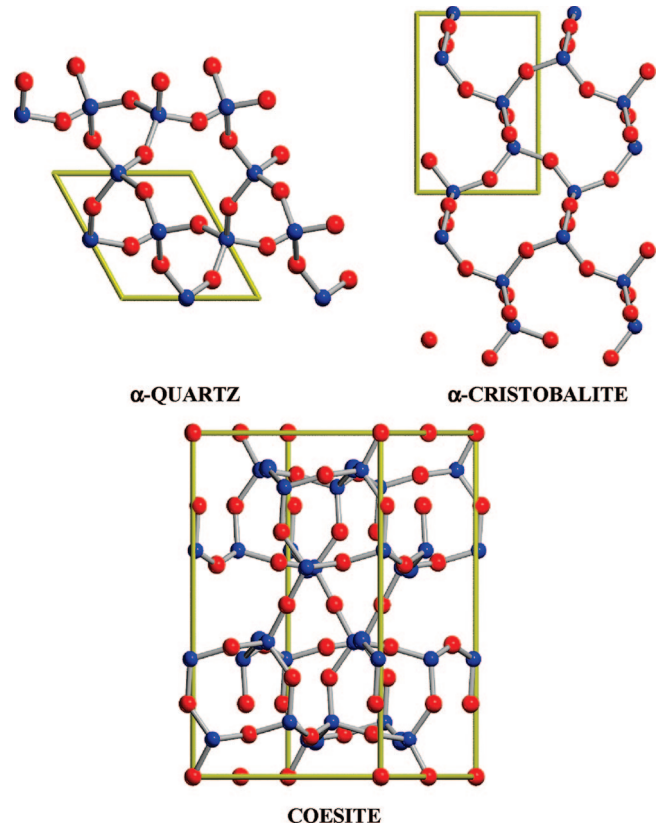

Figure 1. Unit cells of α-quartz,[34] α-cristobalite,[35] and coesite.[36] Light blue spheres represent Si and light red spheres represent O. Manipulation and visualization of structures have been dealt with the MOLDRAW program,[24] and molecular drawings have been rendered by the POVRAY program using input files prepared with MOLDRAW.

All the investigated silica polymorphs consist of three-dimensional SiO_4 tetrahedral networks but have different tetrahedral connectivity. In the structure of α-quartz and α-cristobalite, the SiO_4 tetrahedra form six-membered rings; each contains only a single Si and a single O site. In the structure of coesite, there are two Si and five O sites: O1 and O2 are part of large six- or eight-membered rings that cross-link the smaller four-membered rings made by O3, O4, and O5. Figure 1 reports the structure of α-quartz, α-cristobalite, and coesite. Sigma-2 and ferrierite are two well-known zeolites whose structures are reported in Figure 2.

Sigma-2 is known to be a clathrasil rather than a zeolite, i.e., it has cages but no channel systems. There are four Si and seven O atoms in the asymmetric unit, which are made up of two cages. The large cage is roughly spherical with a free diameter of 7.5 Å and $\bar{4}$ point symmetry. It can be visualized as a tennis ball with twelve five-rings forming the seam and rows of four six-rings filling in the spaces. There are four large cages and eight small ones per unit cell. The small cage consists of three four-rings and six five-rings. Although the structure of Sigma-2 is interesting in its own right, it is used here as a test case because both the structure and the ^{29}Si chemical shift tensor have been recently resolved with good accuracy.[22,23]

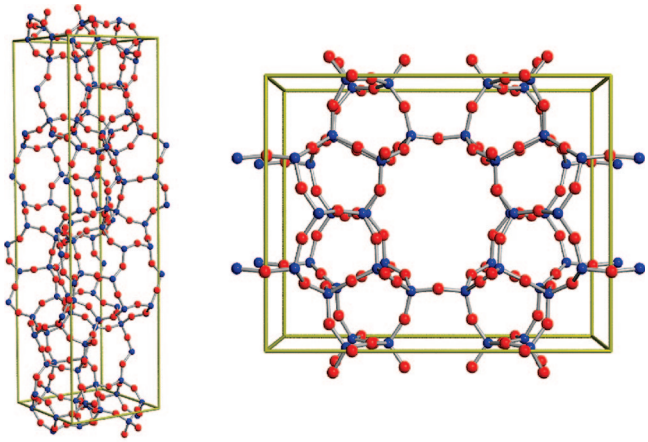

Figure 2. Unit cells of Sigma-2[22] and ferrierite[37] all-silica zeolites.

Ferrierite (FER)[41] is known to be a natural as well as a synthetic material with a framework structure of corner-sharing tetrahedral $TO_{4/2}$ units ($T=Si^{IV}$, Al^{III}) that give a fully condensed 3D framework that contains a system of intersecting channels, circumscribed by 8 T atoms and 10 T atoms.[37,42,43] The aluminum-containing phase has shown potential as a deNOx catalyst for car exhaust systems[44] and is an excellent shape-selective catalyst for the isometization of n-butenes to isobutenes.[45] The latter is an important feedstock for the production of methyl tert butyl ether (MTBE), which is a commercial oxygenate additive in motor fuel.

Methods and Computational Details

Experimental NMR chemical shifts are related to the magnetic shielding tensors, which account for the local electronic environment surrounding the NMR-active nuclei. The nuclear magnetic shielding tensor is expressed as a mixed second derivative of the energy with respect to the external magnetic field, **B**, and the magnetic moment of nucleus X, $\boldsymbol{\mu}^X$

$$\sigma_{ij}^X = \left[\frac{\partial^2 E}{\partial \mu_i^X \partial B_j}\right] \quad (1)$$

where i and j are the components of the nuclear induced magnetic moment and the external magnetic field, respectively. The isotropic shielding constant (σ) is defined as one-third of the trace of the shielding tensor; the chemical shift δ is computed as

$$\delta_{\text{sample}} = \delta_{\text{ref}} + \sigma_{\text{ref}} - \sigma_{\text{sample}} \quad (2)$$

where δ_{sample} and σ_{sample} refer to the compound under study, δ_{ref} is the experimental chemical shift for a suitable reference system, and σ_{ref} is the corresponding computed isotropic shielding.

The calculations of ^{29}Si and ^{17}O shielding tensors were performed with the Gaussian code[46] via the gauge-including atomic orbital (GIAO) approach,[47] which uses basis functions that have and explicit field dependence, as first proposed by Ditchfield.[48] The electronic degrees of freedom were described at different levels of theory: from Hartree−Fock (HF) to Density Functional Theory (DFT). In particular, we exploited the PBE, [29,30] PBE0,[31] B3LYP,[26,27] CAM-B3LYP,[32] and M05−2X[33] exchange-correlation density functional models. The 6−311+G(2df,p) basis set was adopted: this triple-ζ basis set augmented with diffuse and polarization functions has been extensively validated in recent literature.[16,17,19,22]

The systems under investigation were several silica polymorphs: α-quartz, α-cristobalite, coesite, Sigma-2, and ferrierite all-silica zeolites. For the purpose of comparing the aforementioned levels of theory, the ^{29}Si and ^{17}O NMR parameters were computed on experimental geometries, thus avoiding subtle indirect effects related to structural relaxation. In order to establish the most accurate and feasible computational procedure, two alternative approaches have been applied to compute the ^{29}Si and ^{17}O shielding constants of α-quartz and α-cristobalite, namely, the *cluster* approach and the hybrid Quantum-Mechanics/Molecular-Mechanics (QM/MM) method, within the ONIOM scheme.[38−40]

The *cluster* approach consists of extracting finite-size models from a given crystal structure: specific clusters are constructed for each crystallographically inequivalent ^{29}Si and ^{17}O sites, with the atom of interest at the center of the structural model made by its coordination shells. Obviously, the computed molecular properties depend to some extent on the size of the cluster model; therefore, the convergence of NMR shielding constants against the number of coordination shells was tested: Si- and O- centered clusters were built up to three complete tetrahedral shells (five complete atomic shells) embedding the site under investigation. In the following these cluster models are referred to as shell-*n*, where *n* denotes the number of complete atomic shells. The geometrical parameters were taken from experimental data: namely, single crystal X-ray or neutron scattering experiments.[22,34−37] Previous studies[14,22] demonstrated that this choice of reference geometries ensures better agreement between computed and experimental chemical shifts than the use of the structural parameters determined by powder X-ray diffraction experiments. Consistently with recent literature,[14,19,21,22,49] the clusters are terminated with H atoms whose positions are kept fixed along the direction of Si−O and O−Si bonds of the parent crystal structure, using O−H and Si−H distance of 0.96 and 1.48 A, respectively. These parameters correspond to the optimum O−H bond length, for non-hydrogen-bonded Si−O−H linkages in various silicate clusters, and to the optimum Si−H bond length, for Si_2OH_6 dimer, as computed at the B3LYP/6−311+G(2df,p) level of theory. In some cases, at the boundary of the cluster, when the atoms of the outer coordination shells form four-membered rings, an additional Si atom has been included together with two terminating H atoms.

Complementary to the cluster approach, the importance of including long-range electrostatic effects when computing the ^{29}Si and ^{17}O shielding tensor has been investigated by making use of the well-known ONIOM method.[38−40] In this framework, the system under study is subdivided into two (or more) regions of concentric layers, each of which is treated at a different level of theory. Following the original

nomenclature proposed by Morokuma,[38−40] the whole system is called the *real system*. The most important part of the system forms the innermost layer, the *model system*, which is described at the highest degree of accuracy: the *model system* usually includes the most chemically relevant portion of the entire system, i.e. the region where the local phenomena of interest take place. Subsequent layers are described with progressively less accurate methods, i.e. lower-level QM models or molecular mechanics. The boundary between the *model system* and the exterior layer could also be along covalent bonds; in this case, the consistency of the model system is attained by adding a set of fictitious atoms, usually H atoms, along the directions of pre-existing chemical bonds. The two-layer scheme has been employed, performing QM/MM computations with the so-called 'electronic embedding' scheme, namely including the point charges of the MM layer in the QM Hamiltonian of the *model system* according to the scheme

$$\hat{H}_{el}(\text{model:MM}) = \hat{H}_{el}(\text{model}) - \sum_{i}^{Y}\sum_{J}^{X}\frac{q_J}{r_{iJ}} \qquad (3)$$

where H_{el}(model:MM) and H_{el}(model) are the electronic Hamiltonians for the QM region with and without the external field, Y is the number of the electrons in the model system, and X is the number of the point charges in the MM region. This scheme allows the QM wave function to be properly polarized by the electrostatic properties of the surroundings.

In our calculations, the *real system* consists of a sphere made of ca. 1200−1300 atoms, which have been extracted from the experimental structures of α-quartz and α-cristobalite with the Si and O sites of interest at the center of each sphere. The outer Si and O atoms have been saturated with OH and H atoms with the Si−O−H angles and O−H bond lengths set to 115.0° and 0.96 Å, respectively. The Unified Force Field (UFF)[50] parameters have been exploited, and the partial atomic charges have been obtained according to the Qeq scheme developed by Rappe and Goddard.[51] Regarding the *model system*, the HF and PBE levels of theory on structures with equivalent shell-*n* size as for the aforementioned cluster approach have been adopted. In order to avoid spurious effects by the electronic embedding, the MM point charges of the atoms at the boundary between *model* and *real systems* have been properly scaled by using the default values set in the Gaussian code.

The dependence of shielding constants both on the Si-centered cluster and *model system* sizes has been tested by using shell-*n* clusters with $n = 1$ (1 Tetrahedron, 1T), 3 (2T), 5 (3T), and 7 (4T) by using the 6−311+G(2d) basis set for the central silicon and oxygen atoms of the first shell, the 6−31+G(d) basis set for the atoms of the second tetrahedron, and the 6−31G* basis set on all the further atoms. Shell-*n* clusters with $n = 1$, 2, 4, and 6 have been used in the case of O-centered clusters.

Besides the ^{29}Si and ^{17}O chemical shifts, the ^{17}O electric field gradients and quadrupolar parameters have been also calculated. The primary quantum-mechanical quantity is the traceless electric field gradient (efg) tensor, whose elements

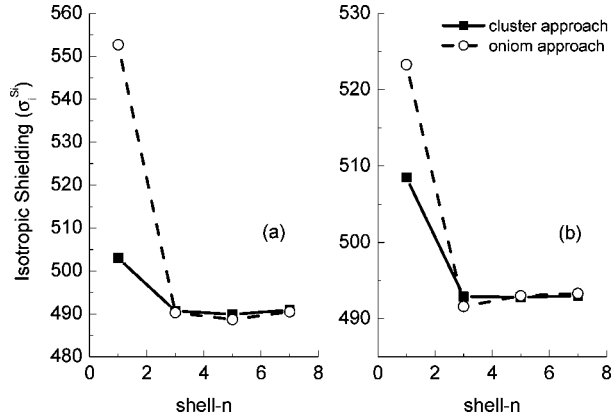

Figure 3. Comparison between ^{29}Si isotropic shielding calculated by using the cluster approach (solid line) and the oniom approach (dashed line) for (a) α-quartz and (b) α-cristobalite as a function of cluster and model system size. High level calculations performed at the Hartree−Fock level of theory by using the 6−311+G(2d) basis set for the central silicon and oxygens of the first shell ($n = 1,2$). The 6−31+G(d) basis set has been used for the atoms of the second shell ($n = 3,4$) and 6−31G* basis set for the atoms of the third shell and beyond ($n > 4$). In the ONIOM approach the low level calculations were performed by using the UFF embedded charges (Qeq scheme).

are related to the quadrupolar coupling constant, C_Q, and quadrupolar coupling asymmetry parameter, η_Q, according to

$$C_q = e^2Q\langle q_{zz}\rangle/h, \text{ and } \eta_Q = \frac{\langle q_{xx}\rangle - \langle q_{yy}\rangle}{\langle q_{zz}\rangle} \qquad (4)$$

where eQ is the nuclear quadrupole moment of the nucleus of interest, and $e\langle q_{xx}\rangle$, $e\langle q_{yy}\rangle$, and $e\langle q_{zz}\rangle$ are the components of the efg tensor at the nucleus in the principal axis system, with $|\langle q_{zz}\rangle| > |\langle q_{yy}\rangle| > |\langle q_{xx}\rangle|$. Since the nuclear quadrupole moment eQ cannot be measured experimentally, it has been usually derived from the experimental C_Q value and the calculated efg of the free atom, ground-state atomic O ($^3P_2$) in the case of ^{17}O. The resultant eQ is thus dependent on the employed level of theory. In order to achieve internal consistency and a better agreement with experimental data, we used an eQ value calculated at the same level as for the studied clusters. Under such circumstances, the eQ values were derived from the accurate experimental ^{17}O C_Q of the H_2O molecule (10.175 ± 0.067 MHz)[52] and the $e\langle q_{zz}\rangle$ values computed for the same water molecule at the same level of theory as that exploited for the silica clusters.

Results and Discussion

^{29}Si NMR. CLUSTER vs ONIOM Performances and System-Size Convergence. Figure 3 reports a comparison between ^{29}Si isotropic shielding calculated by using the cluster approach (solid line) and the ONIOM approach (dashed line) for representative Si sites (namely, α-quartz and α-cristobalite) as a function of cluster and model system size. The high level calculations (cluster approach and model system in the ONIOM approach) were performed at the HF level of theory. In the ONIOM approach the low level

Table 1. Calculated ^{29}Si Isotropic Chemical Shift for Shell-3 Cluster Models of Various SiO_2 Polymorphs Using Different Methods[a]

	HF	B3LYP	PBE0	M05	CAM-B3LYP	exp.[b]	Profeta et al.[28]
				Cristobalite			
Si	−109.1 (0.6)	−108.9 (0.4)	−108.9 (0.4)	−109.3 (0.8)	−109.3 (0.8)	−108.5	−109.1 (0.6)
				Coesite			
Si1	−113.6 (0.3)	−115.0 (1.1)	−114.9 (1.0)	−114.0 (0.1)	−114.5 (0.6)	−113.9	−114.7 (0.8)
Si2	−108.7 (0.6)	−109.8 (1.7)	−109.8 (1.7)	−109.0 (0.9)	−109.4(1.3)	−108.1	−108.4 (0.3)
				Sigma2			
Si1	−115.2 (0.6)	−117.8 (2.0)	−115.5 (0.3)	−115.9 (0.1)	−117.3 (1.5)	−115.8	
Si2	−113.2 (0.4)	−114.7 (1.1)	−112.3 (1.3)	−114.1 (0.5)	−114.7 (1.1)	−113.6	
Si3	−119.0 (0.7)	−121.2 (1.5)	−118.8 (1.1)	−119.3 (0.4)	−121.0 (1.3)	−119.7	
Si4	−108.9 (0.4)	−110.4 (1.9)	−108.3 (0.2)	−109.6 (1.1)	−110.3 (1.8)	−108.5	
				Ferrierite			
Si1	−116.3 (0.2)	−119.9 (3.4)	−119.3 (2.8)	−117.7 (1.2)	−119.3 (2.8)	−116.5	−117.7 (1.2)
Si2	−112.5 (0.2)	−116.9 (4.6)	−116.1 (3.8)	−114.2 (1.9)	−115.5 (3.2)	−112.3	−113.7 (1.4)
Si3	−112.1 (0.2)	−114.0 (2.1)	−113.7 (1.8)	−112.7 (0.8)	−113.7 (1.8)	−111.9	−112.2 (0.3)
Si4	−117.4 (0.2)	−121.2 (4.0)	−120.7 (3.5)	−118.8 (1.6)	−120.4 (1.6)	−117.2	−119.5 (2.3)
Si5	−116.1 (0.1)	−119.2 (3.0)	−118.7 (2.5)	−117.1 (0.9)	−118.5 (0.9)	−116.2	−116.3 (0.1)
$<\Delta\delta>$	0.4	2.2	1.7	0.9	1.8		0.9

[a] The 6-311+G(2df,p) basis set has been applied to all atoms. The Si sites in α-quartz,[34] α-cristobalite,[35] coesite,[36] Sigma-2,[22] and ferrierite[37] all-silica zeolites have been cut out from the experimental framework structures. The errors between experimental and calculated data are reported in brackets. [b] Experimental ^{29}Si NMR data taken from ref 3 for cristobalite and coesite, ref 22 for Sigma-2, and ref 37 for ferrierite.

calculations were performed by using the UFF embedded charges (Qeq scheme).[51] The results clearly show that the ^{29}Si isotropic shielding (σ_i^{Si}) converges when three complete atomic shells around Si are included (shell-3 cluster), with a scattering among the values for the shell-3 and shell-7 clusters of only 0.2 ppm for both α-quartz and α-cristobalite. In agreement with these results, Xue et al.[19] compared the calculated σ_i^{Si} for Si-centered shell model clusters of increasing size for cristobalite and coesite (Si1 site) and found that convergence occurred at the shell-3 cluster model, by using the 6−311+G(2df,p) basis set. The same was found by Brouwer et al.[22] by using the 6−311G(2df) basis set on Si-centered clusters of α-quartz.

Figure 3 also shows that computed ^{29}Si isotropic shielding is not really affected by long-range Coulomb interactions included by the ONIOM(QM:MM) approach. Indeed, the scattering values of the shell-7 model are within 0.3−0.4 ppm.

Our results demonstrate that large errors arise from small-sized cluster/model systems, due to the lack of Pauli repulsion and magnetic susceptibility of the nearby atoms in the QM/MM calculations. These QM effects could not be safely described by electrostatic potentials, and quite large systems should be accounted for in the QM calculations of shielding tensors. Therefore, provided that the cluster sizes are sufficiently large, the use of cluster models for QM calculations of the ^{29}Si shielding tensor is relatively accurate, and a QM/MM scheme is not particularly helpful in reducing the computational effort.

^{29}Si NMR. Chemical Shifts. Table 1 lists the ^{29}Si NMR chemical shifts predicted by HF together with those computed by DFT, with B3LYP, PBE0, M05−2X, and CAM-B3LYP density functionals. Calculations of ^{29}Si NMR chemical shifts of different Si sites in α-quartz,[34] α-cristobalite,[35] coesite,[36] Sigma-2,[22] and ferrierite[37] all-silica zeolites have been performed using the shell-3 clusters (see Figures S1, S2, and S3 in the Supporting Information for pictures of the clusters) using α-quartz as secondary chemical shift standard. The experimentally observed isotropic chemical shift for α-quartz referred to tetramethylsilane (TMS) was δ_{iso}^{TMS}(α-quartz) = −107.4 ppm.[53] The calculated shielding values for σ_{iso}(α-quartz) were 491.68, 446.83, 452.94, 444.20, and 446.18 ppm for HF, B3LYP, PBE0, M05−2X, and CAM-B3LYP methods, respectively. The chemical shifts reported in Table 1 have been compared with experimental data and chemical shifts calculated by Profeta et al.[28] by using the PBE density functional and the periodic approach implemented in the PARATEC code.[54] In this approach the gauge including projector augmented wave (GIPAW) method[55] ensures the reproduction of all electron results using pseudopotentials and plane-waves basis sets.

The computed ^{29}Si chemical shifts in closest agreement with experiments are those obtained by HF: the average errors ($<\Delta\delta>$) on the ^{29}Si NMR chemical shifts are 0.4, 2.2, 1.7, 0.9, and 1.8 ppm for HF, B3LYP, PBE0, M052X and CAM-B3LYP, respectively. The largest errors are 0.7, 4.6, 3.8, 1.9, and 3.2 ppm for HF, B3LYP, PBE0, M05−2X, and CAM-B3LYP, respectively. The HF-cluster approach is of even superior accuracy than the GIPAW-PBE periodic approach;[28] the latter having $<\Delta\delta>$ = 0.9 ppm and the largest error equal to 2.3 ppm, in line with the performances of the density-functionals here exploited.

Figures 4 and 5 compare the results of the shell-3 HF/6−311+G(2df,p) calculations of the ^{29}Si chemical shifts with the experimental spectra for Sigma-2 and ferriereite all-silica zeolites, respectively. The assignments according to the experimental structures of Brouwer et al.[22] for Sigma-2 and Lewis et al.[37] for ferrierite are also given above each peak, and the heights of the peaks reflect the multiplicities of each of the sites. It is worth noting that while Sigma-2 has four crystallographic unique Si sites well resolved in the experimental spectrum, ferrierite has five crystallographic unique sites where Si1 and Si5 are separated in the experimental NMR spectrum by only 0.2 ppm. Such a feature has been

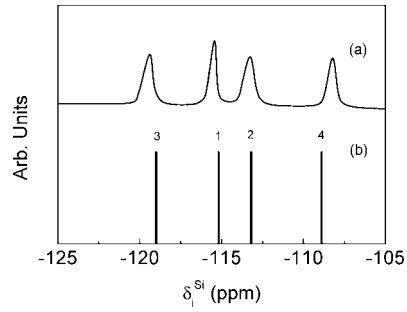

Figure 4. The experimental ^{29}Si NMR isotropic chemical shifts (a) of Sigma-2 taken by Brouwer[23] compared with the (b) calculated shifts (HF/6−311+G(2df,p) with shell-3 Si-centered clusters) of the experimental crystal structure. The numbering scheme corresponds to the Si sites in the crystal structure of Sigma-2.[65]

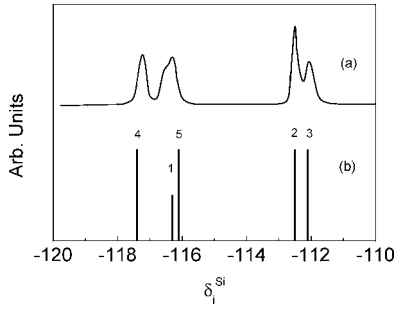

Figure 5. The experimental ^{29}Si NMR isotropic chemical shifts of (a) Sil-ferrierite taken by Lewis[37] compared with the (b) calculated shifts (HF/6−311+G(2df,p) with shell-3 Si-centered clusters) of the experimental crystal structure. The numbering scheme corresponds to the Si sites in the crystal structure of Sil-ferrierite.[37]

remarkably well described by our calculations, and it was not predicted by recent calculations reported by Bull et al.,[14] where an overlap of sites 1 and 5 was found, while a lower accurate shift of 1.3 ppm was obtained by the GIPAW-PBE periodic approach.[28]

A meaningful test for the accuracy of *ab initio* calculations consists of comparing the computed principal components, the span (Ω) and skew (κ) values of the ^{29}Si chemical shift tensor. These quantities can be extracted from recoupling and slow MAS experiments.[22] The principal components of the ^{29}Si chemical shift tensor are the eigenvalues, with $\delta_{11} > \delta_{22} > \delta_{33}$. The span ($\Omega$) describes the breadth of the tensor and the skew (κ) describes the asymmetry of tensor components and are defined as follows

$$\Omega = \delta_{11} - \delta_{33}, \text{ and } \kappa = 3(\delta_{22} - \delta_{iso})/\Omega \qquad (5)$$

where $\delta_{iso} = (\delta_{11}+\delta_{22}+\delta_{33})/3$.

Table 2 lists the principal components, the span (Ω) and skew (κ) values of the ^{29}Si chemical shifts tensor of Sigma-2 calculated at the HF, B3LYP, PBE0, M05−2X, and CAM-B3LYP levels of theory, together with those determined by recoupling and slow MAS experiments.[22] Slow MAS data are more accurate (smaller experimental uncertainties) and are taken as reference in Figure 6 where correlation plots between calculated and observed principal components of the ^{29}Si chemical shifts tensor of Sigma-2 are reported. The average errors of computed principal components are 0.6, 1.9, 1.6, 1.0, and 1.7 ppm for HF, B3LYP, PBE0, M05−2X, and CAM-B3LYP, respectively. A more detailed analysis shows that while HF well reproduces all the trends of the principal components, B3LYP, PBE0, and CAM-B3LYP wrongly predict that δ_{11}(Si4) > δ_{11}(Si2) and δ_{33}(Si2) > δ_{33}(Si3), and the M05−2X method wrongly predicts that δ_{33}(Si2) > δ_{33}(Si3). An even poorer agreement with experiment has been found in the case of the span (Ω) and skew (κ) values (see Figure 7 and Table 2). However, it is worth noting the presence of high experimental uncertainties: different techniques yield quite dissimilar values.

The excellent agreement with the experiments indicates that the HF level of theory on cluster models extracted from the highest quality crystal structures is adequate for calculating ^{29}Si shielding tensors in zeolites and silica polymorphs.

^{17}O NMR. CLUSTER vs ONIOM Performance and System-Size Convergence. Figure 8 reports the ^{17}O isotropic shielding constants calculated by using the cluster approach (solid line) and the ONIOM approach (dashed line) for the single O site of α-cristobalite as a function of cluster and model system size. The high level calculations (cluster approach and model system in the ONIOM approach) were performed at the PBE level of theory by using the 6−311+G(2d) basis set for the central oxygen and silicon of the first two atomic shells ($n = 1,2$) and the 6−31+G(d) basis set for the remaining atoms ($n > 2$). In the ONIOM approach the low level calculations were performed by using the UFF embedded charges (Qeq scheme),[51] in close resemblance with the calculations carried out in the case of ^{29}Si.

The results clearly show that within the cluster approach the ^{17}O isotropic shielding (σ_i^O) converges when four complete atomic shells around O are included (shell-4 cluster), with a scattering among the values for the shell-4 and shell-6 clusters of only 0.3 ppm. Figure 8 also shows that σ_i^O is slightly affected by long-range Coulomb interactions, as included in the ONIOM approach, even though not in a systematic way. However, since the shell-6 model system contains more than 130 atoms a further expansion of the cluster size would require too high computational effort. Moreover, in such circumstances the simplest cluster approach would be preferred since the ONIOM approach is usually applied with the aim of decreasing the size of the system to be included in QM calculations.

Table 3 lists the principal components of the electric field gradients calculated for the O-site in α-cristobalite. Our results clearly show that the electric field gradients are not affected by long-range Coulomb interactions and they converge at the shell-4 model size.

^{17}O NMR. Chemical Shifts. The calculations of ^{17}O NMR chemical shifts were performed on shell-4 cluster models of α-quartz,[34] α-cristobalite,[35] and coesite[36] by using the 6−311+G(2df,p) basis set. In the present study, α-cristobalite, δ_{iso}^{H2O}(α-cristobalite) = 40 ± 2 ppm,[56] has been used as internal secondary chemical shift reference: the computed values for σ_{iso}(α-cristobalite) were 272.0, 241.8, 244.2, 238.0, and 233.1 ppm for HF, B3LYP, PBE0, M05−2X, and PBE methods, respectively. These absolute values can be com-

Table 2. Experimental and Calculated Principal Components of the ^{29}Si Chemical Shift Tensors, Span Ω, and Skew κ Values of Sigma-2

site	δ_{11} (ppm)	δ_{22} (ppm)	δ_{33} (ppm)	Ω (ppm)	κ
			Experiment (CSA Recoupling)		
Si1	−108.9 ± 1.1	−113.0 ± 1.0	−125.3 ± 1.1	16.4 ± 1.2	0.50 ± 0.12
Si2	−104.5 ± 1.5	−113.3 ± 1.2	−123.0 ± 1.5	18.5 ± 1.6	0.05 ± 0.18
Si3	−115.3 ± 1.4	−119.6 ± 0.9	−124.1 ± 1.4	8.8 ± 1.7	0.03 ± 0.25
Si4	−103.5 ± 0.9	−105.8 ± 0.9	−116.2 ± 0.9	12.6 ± 0.8	0.65 ± 0.14
			Experiment (Slow MAS)		
Si1	−108.1 ± 0.5	−113.5 ± 0.5	−125.8 ± 0.5	17.7 ± 0.5	0.39 ± 0.06
Si2	−104.3 ± 0.6	−112.8 ± 0.5	−123.6 ± 0.6	19.3 ± 0.6	0.12 ± 0.05
Si3	−114.4 ± 0.3	−119.6 ± 0.3	−125.0 ± 0.3	10.7 ± 0.2	0.02 ± 0.05
Si4	−102.8 ± 0.7	−106.0 ± 0.8	−116.7 ± 0.7	14.0 ± 0.5	0.53 ± 0.13
			Hartree−Fock		
Si1	−107.9	−113.5	−124.2	16.3	0.31
Si2	−103.1	−112.9	−123.7	20.6	0.05
Si3	−114.7	−118.1	−124.0	9.3	0.27
Si4	−102.7	−106.4	−117.5	14.8	0.50
			B3LYP		
Si1	−110.0	−115.9	−127.6	17.6	0.33
Si2	−102.9	−113.8	−127.4	24.5	0.11
Si3	−116.1	−120.3	−127.3	11.2	0.25
Si4	−103.8	−107.6	−119.9	16.2	0.53
			PBE0		
Si1	−109.8	−115.6	−127.1	17.3	0.33
Si2	−102.8	−113.5	−126.8	24.0	0.11
Si3	−115.9	−119.9	−126.6	10.7	0.25
Si4	−103.7	−107.5	−119.7	16.0	0.53
			M052X		
Si1	−108.4	−114.0	−125.3	16.9	0.34
Si2	−102.8	−113.4	−126.1	23.3	0.09
Si3	−114.7	−118.1	−125.0	10.3	0.34
Si4	−102.5	−107.3	−118.9	16.4	0.41
			CAM-B3LYP		
Si1	−109.5	−115.3	−127.2	17.6	0.34
Si2	−103.0	−114.2	−127.0	24.0	0.07
Si3	−116.0	−120.1	−126.9	10.9	0.25
Si4	−103.7	−107.4	−119.7	16.0	0.54

pared with the estimated value of the experimental absolute shielding of 248 ± 2 ppm, obtained from the aforementioned isotropic chemical shift, δ_{iso}^{H2O}(α-cristobalite), and the reported absolute shielding value of 324 ppm for water molecule,[57] plus the shift difference of −36 ppm required to reference molecular to liquid water.[58] The experimental ^{17}O NMR isotropic chemical shift of gaseous water compares fairly well with its theoretical counterpart, as computed at different levels of theory on the experimental structure of gas-phase water (R(O−H)=0.9572 Å and ∠HOH = 104.52°).

These results are listed in Table 4 together with the efg, the ^{17}O efg asymmetry parameter (η) for water and the nuclear quadrupole moment eQ values, derived from the

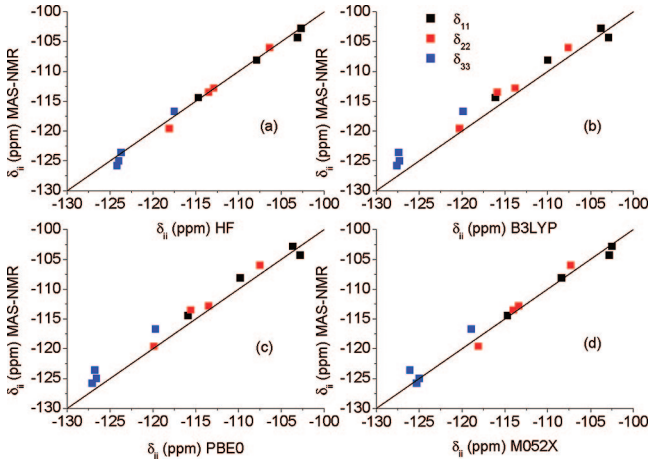

Figure 6. Correlation plots between the experimental (slow MAS experiments) principal components of ^{29}Si chemical shift tensors and the calculated ones at the (a) Hartree−Fock, (b) B3LYP, (c) PBE0, and (d) M052X level of theory for Sigma-2. If the experimental data were perfectly reproduced, the data points would lie on the solid lines (ideal lines of equation $y = x$).

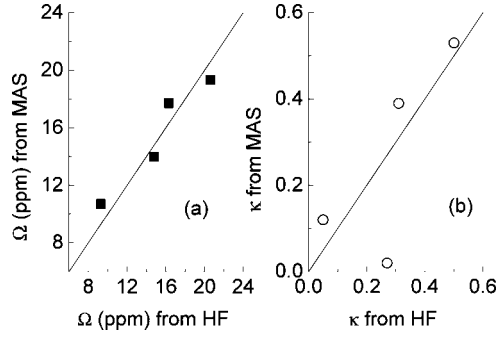

Figure 7. Comparison of (a) the span (Ω) and (b) the skew κ values determined from slow MAS experiments[22] and the ones calculated by the HF/6−311+G(2df,p) method on shell-3 cluster models of Si sites in Sigma-2.

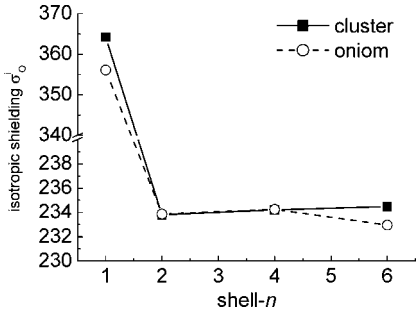

Figure 8. Comparison between ^{17}O isotropic shielding calculated by using the cluster approach (solid line) and the oniom approach (dashed line) for α-cristobalite as a function of cluster and model system size. High level calculations performed at the Hartree−Fock level of theory by using the 6−311+G(2d) basis set for the central oxygen and silicon atoms of the first two atomic shells ($n = 1,2$). The 6−31+G(d) basis set has been used for the atoms of the third shell and beyond ($n > 2$). In the ONIOM approach the low level calculations were performed by using the UFF embedded charges (Qeq scheme).

Table 3. Electric Field Gradients of the O-Site of α-Cristobalite As a Function of System Size within the Cluster and ONIOM Approaches

	$e\langle q_{xx}\rangle$ (au)		$e\langle q_{yy}\rangle$ (au)		$e\langle q_{zz}\rangle$ (au)	
	Cluster	ONIOM	Cluster	ONIOM	Cluster	ONIOM
shell-2	0.418308	0.418271	0.572242	0.572290	−0.99055	−0.99056
shell-4	0.416158	0.416228	0.566511	0.566386	−0.98267	−0.98261
shell-6	0.425327	0.420848	0.511205	0.563811	−0.98493	−0.98466

accurate experimental ^{17}O C_Q of the H_2O molecule (10.175 ± 0.067 MHz)[52] and the $e\langle q_{zz}\rangle$ values computed for the same water molecule at the same levels of theory as those exploited for the silica clusters. The computed η values for water are in the range between 0.80 and 0.76, which compares well with the experimental value of 0.75 ± 0.01 determined by Verhoeven et al.[52] Good agreement is also found for the nuclear quadrupole moment eQ, which ranges between 2.38E-30 and 2.53E-30 m^2 with respect to the experimental value of 2.55E-30 m^2 determined by Pyykko.[59]

Table 5 summarizes the ^{17}O NMR parameters computed by HF, B3LYP, PBE0, M05−2X, and PBE methods for various shell-4 O-centered clusters (see Figures S4 and S5 of the Supporting Information for the pictures of the cluster models used). Moreover, Figure 9 displays a comparison of the calculated C_Q^O with experimental data. The best correlation is found with B3LYP, which reproduces the quadrupolar coupling constant by an average error of 0.04 MHz, with respect to the average error of 0.14, 0.11, 0.36, and 0.10 MHz for HF, PBE0, M05−2X, and PBE, respectively. However, a more in-depth analysis shows that while the PBE method well reproduces all the trends of the C_Q^O of coesite, both B3LYP and PBE0 wrongly predict that $C_Q^O(O2) = C_Q^O(O3)$, and both HF and M05−2X as well as the GIPAW-PBE periodic approach[28] wrongly predict that $C_Q^O(O2) > C_Q^O(O3)$. The calculated η_Q^O values show a reasonable agreement of all the methods with experiments (mostly within 0.05), see Figure 10 and Table 4. The reported deviations fall well within the uncertainties of experimental estimations.

The agreement between calculations and experiments observed in the relative ^{17}O chemical shifts among different oxygen sites is not as good as that for δ_i^{Si}. Indeed, the average errors ($\langle\Delta\delta\rangle$) of computed δ_i^O are 5.7, 4.5, 4.4, 4.7, and 3.9 ppm for HF, B3LYP, PBE0, M05−2X, and PBE methods, respectively; the largest errors being 9.8, 8.4, 7.8, 7.1, and 7.4 for HF, B3LYP, PBE0, M05−2X, and PBE, respectively.

A closer examination of the results listed in Table 5 suggests that our calculations reproduce well the relative δ_i^O for O1 and O2 sites of coesite, with differences between computed and measured values well below the experimental uncertainties of 1 ppm. Both these sites link neighboring four-membered rings. The worse results are obtained for the O3, O4, and O5 sites, all of which are part of four-membered rings. Figure S5 of the Supporting Information shows the exploited coesite shell-4 O centered cluster structures. These have been cut out from the bulk structure (reported in Figure 1) by following the bond connectivity. However, in this way the central oxygen does not feel the effects of the atoms towering above, which are about 3 Å faraway. Thereafter, the low accuracy of predicted δ_i^O values for O3, O4, and O5 sites seems to result from the convergence of cluster size, which is not fulfilled in these cases. To further support such a statement, further calculations on the O4 site (which shows errors between 6.6 and 8.2 ppm depending on the method used) have been performed by using two bigger clusters, namely, the shell-6 cluster (132 atoms) made by the bond connectivity method and a new cluster containing 147 atoms made by including atoms inside a spherical region with a radius of about 7.0 Å (see Figure S6 of the Supporting Information). The results listed in Table 6 show that a shell-4 and a shell-6 O4 clusters of coesite do not reach convergence; the cluster system containing 147 atoms provides the best results compared to experiment, with an error on isotropic chemical shift of only 1 ppm at the PBE/6−311+G(2df,p) level of theory.

In conclusion, these results show that oxygens in some silicate topologies present some difficulties to reach full convergence with respect to the cluster size. Preliminary tests on crystal silicates containing alkali and alkaline-earth cations performed in our laboratories showed that the problem of the convergence of ^{29}Si and ^{17}O NMR parameters with respect to the cluster size is even worse than in SiO_2 polymorphs. This could be probably the reason why previous calculations of ^{29}Si-, ^{27}Al-, and ^{17}O NMR chemical shifts of silicate and alumino-silicate glasses yielded quite poor results.[17,60−62]

Concluding Remarks

In the present paper a comparative study on the performance of quantum chemical techniques in computing the magnetic parameters of SiO_2 polymorphs has been reported. Several all silica systems (α-quartz, α-cristobalite, coesite, Sigma-2, and ferrierite zeolites) and several *ab initio* methods (HF, B3LYP, CAM-B3LYP, PBE, PBE0, and M05−2X) have been tested.

Table 4. ^{17}O Isotropic Shielding (σ_i^O), Diagonal Element of the Electric Field Gradient Tensor ($<q_{ii}>$), Electric Quadrupole Moment of the Oxygen Nucleus Calculated by Using the Experimentally Quadrupolar Coupling Constants of Oxygen in Water ($C_Q^O = 10.175 \pm 0.067$ MHz), and the Asymmetry Parameter for Water Calculated at Different Levels of Theory

	σ_i^O (ppm)	$e<q_{xx}>$ (au)	$e<q_{yy}>$ (au)	$e<q_{zz}>$ (au)	eQ (m^2)	η_Q^O
HF	328.2	−0.179811	−1.642521	1.822333	2.38E-30	0.802658
B3LYP	326.9	−0.200025	−1.566409	1.766434	2.45E-30	0.773527
PBE0	329.3	−0.192725	−1.543946	1.736671	2.49E-30	0.778052
M05−2X	338.8	−0.172313	−1.575157	1.74747	2.48E-30	0.802786
PBE	328.5	−0.201431	−1.512331	1.713762	2.53E-30	0.764925

Table 5. Calculated ^{17}O Isotropic Chemical Shift and EFG Parameters for OH Ended 2T Shell Clusters Models (4 Atomic Shells around Each O Center) of Various SiO_2 Polymorphs Using Different Methods[a]

O site	HF	B3LYP	PBE0	M052X	PBE	exp.	Profeta et al.
				δ_i^O (ppm)			
coesite							
O1	29.7	28.5	28.1	26.1	28.3	29 ± 1	25.8
O2	39.7	40.3	40.1	39.2	41.0	41 ± 1	39.2
O3	47.2	48.6	49.2	49.9	49.5	57 ± 1	56.0
O4	44.8	45.7	46.2	45.9	46.4	53 ± 1	52.4
O5	49.4	51.6	52.4	53.3	53.1	58 ± 1	57.8
cristobalite	40	40	40	40	40	40 ± 2	39.3
quartz	42.5	43.3	43.5	44.2	43.8		44.3
$\Delta\delta$	5.7	4.5	4.4	4.7	3.9		1.4
				C_Q^O (MHz)			
coesite							
O1	5.89	6.04	6.17	5.67	6.15	6.05 ± 0.05	6.24
O2	5.30	5.43	5.53	5.08	5.51	5.43 ± 0.05	5.56
O3	5.28	5.43	5.53	5.05	5.52	5.45 ± 0.05	5.45
O4	5.41	5.56	5.66	5.19	5.66	5.52 ± 0.05	5.73
O5	5.11	5.25	5.34	4.88	5.33	5.16 ± 0.05	5.23
cristobalite	5.11	5.25	5.35	4.87	5.34	5.3 ±0.1	5.30
quartz	5.16	5.28	5.38	4.91	5.36		5.31
ΔC_Q	0.14	0.04	0.11	0.36	0.10		0.10
				η_Q^O			
coesite							
O1	0.013	0.012	0.011	0.014	0.011	0.000 ± 0.005	0.040
O2	0.128	0.121	0.121	0.110	0.118	0.166 ± 0.005	0.190
O3	0.171	0.159	0.157	0.149	0.153	0.168 ± 0.005	0.190
O4	0.136	0.125	0.125	0.122	0.121	0.169 ± 0.005	0.166
O5	0.286	0.274	0.272	0.265	0.269	0.292 ± 0.005	0.296
cristobalite	0.129	0.127	0.128	0.117	0.128	0.125 ± 0.005	0.145
quartz	0.169	0.169	0.171	0.159	0.171		0.202
$\Delta\eta_Q$	0.016	0.022	0.022	0.029	0.025		0.019

[a] The 6-311+G(2df,p) basis set has been applied to all atoms.

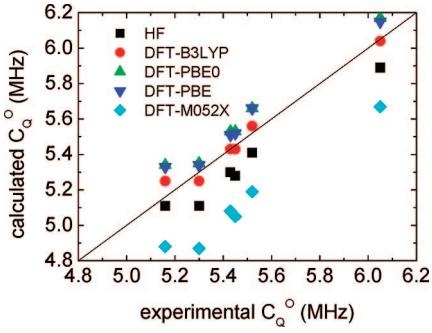

Figure 9. Calculated ^{17}O quadrupolar coupling constants, C_Q^O, for shell-4 O-centered clusters of α-cristobalite and coesite vs experimental values.

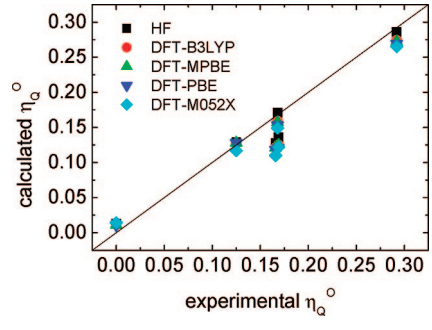

Figure 10. Calculated ^{17}O electric field gradient asymmetry parameter, η_Q^O, for shell-4 O-centered clusters of α-cristobalite and coesite vs experimental values.

First, we consider the convergence of computed parameters with respect to cluster size, with and without the inclusion of partial atomic charges, by the ONIOM(QM:MM) scheme, to account for long-range Coulomb interactions. In the case of ^{29}Si, the computed shielding constants converged at system sizes still amenable to full QM descriptions. Unfortunately, the situation is not the same for ^{17}O parameters: the results show that full convergence is system dependent; in particular, it is hard to achieve for oxygen atoms that are part of small n-membered rings ($n < 6$). However, from our work it is at least evident that the inclusion of long-range electrostatic effects is not mandatory for well-behaving systems and not

Table 6. DFT-PBE//6-311+G(2df) Calculated ^{17}O Isotropic Chemical Shift and efg Parameters for the O4 Site in Coesite as a Function of the Cluster Size Dimension[a]

	shell-4	shell-6	cluster-147 atoms	exp.
σ_i^O	226.65	223.65	219.06	–
δ_i^O (ppm)	46.43	49.43	54.02	53 ± 1
C_Q^O (MHz)	5.66	5.74	5.82	5.52 ± 0.005
η^O	0.1214	0.1861	0.160	0.169 ± 0.005

[a] See Figure S6 of the Supporting Information for pictures of the clusters used.

useful for those systems whose convergence is questionable. Use of QM:QM embedding techniques[63] or periodic boundary conditions[64] seem to be viable solutions for the systems whose complexity prevent the safe cutting out of cluster models.

Regarding the quality of our results, an excellent agreement with experiments has been found for the ^{29}Si chemical shifts of Sigma-2 and ferrierite zeolites. In this second case, the characteristic features of the experimental spectrum have been predicted with an accuracy that has never been achieved before.

In conclusion, the present work shows that the HF model could be safely exploited for computing ^{29}Si magnetic parameters, while methods rooted into DFT perform slightly better in the more complex case of ^{17}O nucleus. It is worth noting that the calculations of magnetic shielding tensors result in being challenging for the currently available density functionals: the slightly better or comparable performance of HF than DFT highlights the importance of developing and testing new exchange-correlation approximations for an accurate prediction of molecular parameters.

Therefore, beyond the intrinsic relevance of the investigated silicate systems, the many theoretical results reported here represent, in our opinion, valuable references for computational chemists approaching the theoretical study of NMR parameters for SiO_2 polymorphs.

Acknowledgment. The authors thank the Italian Ministry of University and Research for funding (Project COFIN2006, Prot. 2006033728 "New computational strategies for modeling nano-structured glasses and their spectroscopic properties"). The large scale computing facilities of the CR-INSTM "Village" network are also acknowledged.

Supporting Information Available: Pictures of all the clusters considered. This material is available free of charge via the Internet at http://pubs.acs.org.

References

(1) Stebbins, J. F. Nuclear magnetic resonance spectroscopy of silicates and oxides in geochemistry and geophysicsIn *Mineral physics and crystallography, a handbook of physical constants*; American Geophysical Union: Washington, DC, 1995; p 303.

(2) Engelhardt, G.; Michel, D. *High-Resolution Solid-State NMR of Silicates and Zeolites*; Wiley: New York, 1987; p 106.

(3) Smith, J. V.; Blackwell, C. S. *Nature* **1983**, *303*, 223.

(4) Engelhardt, G.; Radeglia, R. *Chem. Phys. Lett.* **1984**, *108*, 271.

(5) Ramdas, S.; Klinowski, J. *Nature* **1984**, *308*, 525.

(6) Janes, N.; Oldfiels, E. *J. Am. Chem. Soc.* **1985**, *107*, 6769.

(7) Oestrike, R.; Yang, W.-H.; Kirkpatric, R. J.; Hervig, R. L.; Navrotsky, A.; Montez, B. *Geochim. Cosmochim. Acta* **1987**, *51*, 2199.

(8) Sherriff, B. L.; Grundy, H. D. *Nature* **1988**, *332*, 819.

(9) Stebbins, J. F.; Kanzaki, M. *Science* **1991**, *251*, 294.

(10) Mauri, F.; Pasquarello, A.; Pfrommer, B. G.; Yoon, Y. G.; Louie, S. G. *Phys. Rev. B* **2000**, *62*, R4786.

(11) Grandinetti, P. J.; Baltisberger, J. H.; Farnan, I.; Stebbins, J. F.; Werner, U.; Pines, A. *J. Phys. Chem.* **1995**, *99*, 12341.

(12) Grandinetti, P. J.; Clark, T. M. *Mod. Magn. Reson.* **2006**, *3*, 1543.

(13) Clark, T. M.; Grandinetti, P. J.; Florian, P.; Stebbins, J. F. *Phys. Rev. B* **2004**, *70*, 064202/1.

(14) Bull, L. M.; Bussemer, B.; Anupold, T.; Reinold, A.; Samoson, A.; Sauer, J.; Cheetham, A. K.; Dupree, R. *J. Am. Chem. Soc.* **2000**, *122*, 4948.

(15) Bull, L. M.; Cheetham, A. K.; Anupold, T.; Reinold, A.; Samoson, A.; Sauer, J.; Bussemer, B.; Lee, Y.; Gann, S.; Shore, J.; Pines, A.; Dupree, R. *J. Am. Chem. Soc.* **1998**, *120*, 3510.

(16) Xue, X.; Kanzaki, M. *Phys. Chem. Miner.* **1998**, *26*, 14.

(17) Xue, X.; Kanzaki, M. *J. Phys. Chem. B* **1999**, *103*, 10816.

(18) Clark, T. M.; Grandinetti, P. J. *J. Phys.: Condens. Matter* **2003**, *15*, S2387.

(19) Xue, X.; Kanzaki, M. *Solid State Nucl. Magn. Reson.* **2000**, *16*, 245.

(20) Azizi, S. N.; Rostami, A. A.; Godarzia, A. A. *J. Phys. Soc. Jpn.* **2005**, *74*, 1609.

(21) Bussemer, B.; Schroder, K.-P.; Sauer, J. *Solid State Nucl. Magn. Reson.* **1997**, *9*, 155.

(22) Brouwer, D. H.; Enright, G. D. *J. Am. Chem. Soc.* **2008**, *130*, 3095.

(23) Brouwer, D. H. *J. Am. Chem. Soc.* **2008**, *130*, 6306.

(24) Civalleri, B.; Garrone, E.; Ugliengo, P. *Chem. Phys. Lett.* **1999**, *299*, 443.

(25) Casanovas, J.; Illas, F.; Pacchioni, G. *Chem. Phys. Lett.* **2000**, *326*, 523.

(26) Becke, A. D. *J. Chem. Phys.* **1993**, *98*, 5648.

(27) Lee, C.; Yang, W.; Parr, R. G. *Phys. Rev. B* **1988**, *37*, 785.

(28) Profeta, M.; Mauri, F.; Pickard, C. J. *J. Am. Chem. Soc.* **2003**, *125*, 541.

(29) Perdew, J. P.; Burke, K.; Ernzerhof, M. *Phys. Rev. Lett.* **1996**, *77*, 3865.

(30) Perdew, J. P.; Burke, K.; Ernzerhof, M. *Phys. Rev. Lett.* **1997**, *78*, 1396.

(31) Adamo, C.; Barone, V. *J. Chem. Phys.* **2002**, *116*, 5933.

(32) Yanai, T.; Tew, D. P.; Handy, N. C. *Chem. Phys. Lett.* **2004**, *393*, 51.

(33) Zhao, Y.; Schultz, E.; Truhlar, D. G. *J. Chem. Theory Comput.* **2006**, *2*, 364.

(34) Will, G.; Bellotto, M.; Parrish, W.; Hart, M. *J. Appl. Crystallogr.* **1988**, *21*, 182.

(35) Schmahl, W. W.; Swainson, I. P.; Dove, M. T.; Graeme-Barber, A. *Z. Kristallogr.* **1992**, *201*, 125.

(36) Smyth, J. R.; Smith, J. V.; Artioli, G.; Kvick, A. *J. Phys. Chem.* **1987**, *91*, 988.

(37) Lewis, J. E.; Freyhardt, C. C.; Davis, M. E. *J. Phys. Chem.* **1996**, *100*, 5039.

(38) Maseras, F.; Morokuma, K. *J. Comput. Chem.* **1995**, *16*, 1170.

(39) Svensson, M.; Humbel, S.; Froese, R. D. J.; Matsubara, T.; Sieber, S.; Morokuma, K. *J. Phys. Chem.* **1996**, *100*, 19357.

(40) Humbel, S.; Sieber, S.; Morokuma, K. *J. Chem. Phys.* **1996**, *105*, 1959.

(41) Meier, W. M.; Olson, D. H. *Atlas of Zeolite Structure Types*; Butterworth-Heinemann: Boston, 1992.

(42) Vaughan, P. A. *Acta Crystallogr.* **1966**, *21*, 983.

(43) Wise, W. S.; Tschernich, R. W. *Am. Mineral.* **1976**, *61*, 60.

(44) Attfield, M. P.; Weigel, S. J.; Cheetham, A. K. *J. Catal.* **1997**, *172*, 274.

(45) Haggin, J. C&EN 1993, October 25, p 30.

(46) Frisch, M. J.; Trucks, G. W.; Schlegel, H. B.; Scuseria, G. E.; Robb, M. A.; Cheeseman, J. R.; Montgomery, J. A., Jr.; Vreven, T.; Kudin, K. N.; Burant, J. C.; Millam, J. M.; Iyengar, S. S.; Tomasi, J.; Barone, V.; Mennucci, B.; Cossi, M.; Scalmani, G.; Rega, N.; Petersson, G. A.; Nakatsuji, H.; Hada, M.; Ehara, M.; Toyota, K.; Fukuda, R.; Hasegawa, J.; Ishida, M.; Nakajima, T.; Honda, Y.; Kitao, O.; Nakai, H.; Klene, M.; Li, X.; Knox, J. E.; Hratchian, H. P.; Cross, J. B.; Bakken, V.; Adamo, C.; Jaramillo, J.; Gomperts, R.; Stratmann, R. E.; Yazyev, O.; Austin, A. J.; Cammi, R.; Pomelli, C.; Ochterski, J. W.; Ayala, P. Y.; Morokuma, K.; Voth, G. A.; Salvador, P.; Dannenberg, J. J.; Zakrzewski, V. G.; Dapprich, S.; Daniels, A. D.; Strain, M. C.; Farkas, O.; Malick, D. K.; Rabuck, A. D.; Raghavachari, K.; Foresman, J. B.; Ortiz, J. V.; Cui, Q.; Baboul, A. G.; Clifford, S.; Cioslowski, J.; Stefanov, B. B.; Liu, G.; Liashenko, A.; Piskorz, P.; Komaromi, I.; Martin, R. L.; Fox, D. J.; Keith, T.; Al-Laham, M. A.; Peng, C. Y.; Nanayakkara, A.; Challacombe, M.; Gill, P. M. W.; Johnson, B.; Chen, W.; Wong, M. W.; Gonzalez, C.; Pople, J. A. *Gaussian03, Revison C.02*; Gaussian, Inc.: Wallingford CT, 2004.

(47) Cheeseman, J. R.; Trucks, G. W.; Keith, T. A.; Frisch, M. J. *J. Chem. Phys.* **1996**, *104*, 5497.

(48) Ditchfield, R. *Mol. Phys.* **1974**, *27*, 789.

(49) Barone, V. *Surf. Sci.* **1987**, *189−190*, 106.

(50) Rappé, A. K.; Casewit, C. J.; Colwell, K. S.; Goddard, W. A., III.; Skiff, W. M. *J. Am. Chem. Soc.* **1992**, *114*, 10024.

(51) Rappe, A. K.; Goddard, W. A. I. *J. Phys. Chem.* **1991**, *95*, 3358.

(52) Verhoeven, J.; Dynamus, A.; Bluyssen, H. *J. Chem. Phys.* **1969**, *15*, 3330.

(53) Magi, M.; Lippmaa, E.; Samoson, A.; Engelhardt, G.; Grimmer, A.-R. *J. Phys. Chem.* **1984**, *88*, 1518.

(54) Pfrommer, B.; Raczkowski, D.; Canning, A.; Louie, S. G. *PARATEC (PARAllel Total Energy Code)*; Lawrence Berkeley National Laboratory: with contributions from Mauri, F. C. M., Yoon, Y., Pickard, C., Haynes, P., Eds.; for more information see www.nersc.gov/projects/paratec. Page last modified: Thu, 03 Jun 2004 21:03:20 GMT.

(55) Pickard, C. J.; Mauri, F. *Phys. Rev. B* **2001**, *63*, 245101.

(56) Spearing, D. R.; Farnan, I.; Stebbins, J. F. *Phys. Chem. Miner.* **1992**, *19*, 307.

(57) Vaara, J.; Lounila, J.; Ruud, K.; Helgaker, T. *J. Chem. Phys.* **1998**, *109*, 8388.

(58) Wasylishen, R. E.; Mooibroek, S.; Macdonald, J. B. *J. Chem. Phys.* **1984**, *81*, 1057.

(59) Pyykko, P. *Mol. Phys.* **2001**, *99*, 1617.

(60) Cody, G. D.; Mysen, B.; Sàghi-Szabò, G.; Tossell, J. A. *Geochim. Cosmochim. Acta* **2001**, *65*, 2395.

(61) Tossell, J. A.; Horbach, J. *J. Phys. Chem. B* **2005**, *109*, 1794.

(62) Tossell, J. A. *Phys. Chem. Miner.* **2004**, *31*, 41.

(63) Huang, P.; Carter, E. A. *J. Chem. Phys.* **2006**, *125*, 084102.

(64) Ferrero, M.; Rerat, M.; Orlando, R.; Dovesi, R. *J. Comput. Chem.* **2008**, *29*, 1450.

(65) McCusker, L. B. *J. Appl. Crystallogr.* **1988**, *21*, 305.

CT8003035